Microscopic Fast-Coupler Realization of Scalar-Selection Closure in Weighted Graph Media

Revised narrow results draft v4: rate closure, clock closure, and protocol dependence

Joshua Farrow
Independent Research

April 2026

Abstract

We develop and test a minimal microscopic fast-coupler model that realizes the weighted graph Laplacian used in scalar-selection closure. The model begins with a specified substrate graph, slow node loads Λ_i, and fast edge variables x_e. In the positive diagonal edge-coupler regime, adiabatic elimination gives

$$L_w = B^T G \Omega^{-1} H B = B^T \operatorname{diag}(w_e) B, \qquad w_e = g_e h_e / \Omega_e > 0,$$

where B is the oriented incidence matrix. Thus the substrate connectivity is specified by the architecture, but the scalar response weights and node-level operator are generated by eliminating microscopic edge degrees of freedom rather than inserted directly at the scalar-response level. Static closure is the Schur complement of the full block system and is verified to machine precision. The nontrivial result is dynamic: for each uniform-fast-scale graph mode λ_n, the full two-sector roots obey

$$(r + \mu^2)(r + \Omega) + \Omega\lambda_n = 0,$$

so the Markovian scalar rate $\tau_n^{-1} \simeq \mu^2 + \lambda_n$ is recovered only in the adiabatic regime. The slow-root rate approaches from above with leading relative correction λ_n/Ω, while finite coupler speed produces predictable memory shifts and underdamped ringing when $(\Omega - \mu^2)^2 < 4\Omega\lambda_n$. We also add a minimal clock channel, $\dot{\phi}_i = \omega_0 + \alpha\Lambda_i$, and show that integrated timing observables probe the static gain rather than the instantaneous modal rate. For zero initial fast-sector excitation, $\int_0^\infty \Lambda_n(t)dt = \Lambda_n(0)/(\mu^2 + \lambda_n)$ for every Ω in the linear model; for pre-equilibrated fast-sector initial conditions, the clock-area error scales as λ_n/Ω. Thus rate closure is the strict dynamic test, while DC/integrated timing closure is robust only for specific low-frequency protocols. Noisy full time-domain integrations of the coupled (Λ, x) system recover the predicted graph-mode behavior, and positive edge-disorder tests show that fitted rates track the new weighted spectra. The result is a microscopic bridge for internal scalar closure, not a derivation of external geometry, gravity, Lorentz invariance, or a tensor/spin-2 sector.

1 Introduction

The scalar-selection program asks whether a structured microscopic medium can present, after coarse graining, a reduced scalar observable sector governed by a single graph operator. In the broader program, the proposed dependency chain is

$$H_{\text{micro}} \longrightarrow W \longrightarrow L_w \longrightarrow d_{\text{eff}} \longrightarrow G_{d_{\text{eff}}}(r) \longrightarrow \Lambda(r) \longrightarrow \omega_{\text{eff}}. \tag{1}$$

The present paper addresses only the first internal steps of this chain. Can a microscopic medium produce the weighted graph Laplacian L_w that appears in scalar closure, and how do the associated scalar and clock observables behave outside the ideal adiabatic regime?

The answer is narrow but useful. We specify a substrate graph whose edges host fast coupler variables. Eliminating those edge variables produces a weighted Laplacian on the slow node loads. This does not derive the substrate graph itself. It is better described as a microscopic realization, or network synthesis, of a positive weighted Laplacian on a specified substrate graph.

The paper then separates three levels of closure:

1. **Static scalar closure:** the steady-state scalar load obeys the Schur-complement equation exactly in the positive diagonal regime.
2. **Dynamic rate closure:** modal decay rates follow $\tau_n^{-1} = \mu^2 + \lambda_n$ only when the fast-coupler scale is large compared with the excited graph modes.
3. **Integrated clock closure:** for a minimal clock law, phase shifts depend on $\int \Lambda dt$ and therefore probe the low-frequency/static gain. This makes timing robust in some protocols but not universally protected.

This distinction is important because scalar-selection is ultimately a timing-first program. A model that only discusses modal relaxation rates has not yet explained why clock observables may be more stable than rate observables. Conversely, a claim that timing is always protected would be too strong. The corrected result is two-tiered: rates reveal finite-coupler memory; DC or integrated clocks can suppress it under the appropriate preparation and measurement protocol.

2 Scalar-selection closure

The leading internal scalar closure is

$$(\kappa L_w + \mu^2 I)\Lambda = A\rho, \tag{2}$$

with $\kappa > 0$, screening scale $\mu \geq 0$, scalar load Λ, and source ρ. Its Markovian dynamical completion is

$$\partial_t \Lambda + \Gamma(\kappa L_w + \mu^2 I)\Lambda = \Gamma A \rho(t). \tag{3}$$

If $L_w \phi_n = \lambda_n \phi_n$, Eq. (3) predicts

$$\tau_n^{-1} = \Gamma(\kappa \lambda_n + \mu^2). \tag{4}$$

For clarity, the simulations below set $\Gamma = \kappa = A = 1$ unless otherwise noted.

There is a zero-mode subtlety. For a connected graph, L_w has the constant null vector. If $\mu = 0$, the static equation is solvable only after imposing source neutrality, projecting away the constant mode, or fixing a gauge/reference level for Λ. In this paper, static comparisons use $\mu^2 > 0$ unless explicitly discussing the weak-screening ratio. Dynamic comparisons focus on first nonzero and higher modes, so the constant mode does not carry the reported relaxation rates.

3 Microscopic fast-coupler model

Let $G_{\text{sub}} = (V, E)$ be an oriented substrate graph with N vertices and M edges. Let $B \in \mathbb{R}^{M \times N}$ be the oriented incidence matrix,

$$B_{ei} = \begin{cases} +1, & i = \text{tail}(e), \\ -1, & i = \text{head}(e), \\ 0, & \text{otherwise.} \end{cases} \tag{5}$$

The orientation is arbitrary; $B^T \operatorname{diag}(w_e) B$ is independent of the chosen orientation for positive edge weights.

We place slow scalar loads $\Lambda \in \mathbb{R}^N$ on vertices and fast variables $x \in \mathbb{R}^M$ on edges:

$$\dot{\Lambda} = -\mu^2 \Lambda - B^T G x + A\rho(t), \tag{6}$$

$$\dot{x} = HB\Lambda - \Omega x. \tag{7}$$

The positive diagonal fast-coupler regime is

$$G = \operatorname{diag}(g_e), \qquad H = \operatorname{diag}(h_e), \qquad \Omega = \operatorname{diag}(\Omega_e), \qquad g_e h_e / \Omega_e > 0. \tag{8}$$

This restriction is essential. If $G\Omega^{-1}H$ is non-symmetric or sign-indefinite, the slow operator may become directed, non-normal, or unstable rather than an ordinary scalar Laplacian.

3.1 Adiabatic elimination and Schur complement

When the edge sector is fast,

$$x \approx \Omega^{-1} HB\Lambda. \tag{9}$$

Substituting into Eq. (6) gives

$$\dot{\Lambda} \approx -\left(\mu^2 I + B^T G \Omega^{-1} HB\right) \Lambda + A\rho(t). \tag{10}$$

Thus

$$L_w = B^T G \Omega^{-1} HB. \tag{11}$$

In the positive diagonal case,

$$w_e = \frac{g_e h_e}{\Omega_e} > 0, \qquad L_w = B^T \operatorname{diag}(w_e) B. \tag{12}$$

The substrate graph is chosen by the medium architecture, but the scalar-response weights and slow-sector operator are generated by microscopic edge parameters.

3.2 Stability in the positive diagonal regime

With $M = G\Omega^{-1}H = \operatorname{diag}(w_e)$ and $w_e > 0$, the generated operator satisfies

$$y^T L_w y = (By)^T M (By) = \sum_{e=(i,j)} w_e (y_i - y_j)^2 \geq 0. \tag{13}$$

Thus L_w is symmetric positive semidefinite, with the constant vector as its only null vector on a connected graph. For $\mu^2 > 0$, the reduced Markovian generator $-(\mu^2 I + L_w)$ is strictly stable.

For constant source, the full microscopic steady state satisfies

$$\begin{bmatrix} -\mu^2 I & -B^T G \\ HB & -\Omega \end{bmatrix} \begin{bmatrix} \Lambda \\ x \end{bmatrix} + \begin{bmatrix} A\rho \\ 0 \end{bmatrix} = 0. \tag{14}$$

Its Schur complement is Eq. (2). Static closure is therefore expected to pass to numerical precision; it is a consistency check, not the main evidence.

4 Dynamic closure and finite-coupler memory

For uniform fast scale Ω and an eigenmode λ_n of the generated L_w, the full two-sector dynamics reduce to

$$(r+\mu^2)(r+\Omega)+\Omega\lambda_n=0. \tag{15}$$

The roots are

$$r_\pm=-\frac{\Omega+\mu^2}{2}\pm\frac{1}{2}\sqrt{(\Omega-\mu^2)^2-4\Omega\lambda_n}. \tag{16}$$

For large Ω, the slow root is

$$r_{\text{slow}}=-(\mu^2+\lambda_n)\left[1+\frac{\lambda_n}{\Omega}+O(\Omega^{-2})\right]. \tag{17}$$

Thus the decay rate approaches the scalar-closure rate from above, and the leading relative rate error is approximately λ_n/Ω. This analytic envelope is the backbone of the rate-error plots below.

If

$$(\Omega-\mu^2)^2<4\Omega\lambda_n, \tag{18}$$

the mode is underdamped, with envelope decay $(\Omega+\mu^2)/2$ and oscillation frequency determined by the imaginary part of Eq. (16). Closure failure is therefore structured: high-λ_n modes ring or show memory effects first.

The compact root formula assumes a uniform fast scale Ω after the weights have been generated. If the same static L_w is produced by two different microscopic triples (G,H,Ω) with nonuniform Ω_e, their steady-state scalar closures can agree while their memory kernels and transient spectra differ. In Laplace space, eliminating the fast variables without taking the adiabatic limit gives

$$\left[sI+\mu^2I+B^TG(sI+\Omega)^{-1}HB\right]\Lambda(s)=A\rho(s)+\text{initial-condition terms}. \tag{19}$$

Only as $s/\Omega_e\to 0$ does this reduce to $sI+\mu^2I+L_w$. Therefore L_w is the correct static and adiabatic operator, but finite-coupler dynamics need not be determined by L_w alone.

5 Clock observables: protected DC gain, not universal protection

To connect the internal scalar load to a timing observable, we add the minimal weak-load clock channel

$$\dot\phi_i=\omega_0+\alpha\Lambda_i. \tag{20}$$

For a projected graph mode $a_n(t)=\phi_n^T\Lambda(t)$, the accumulated phase shift is

$$\Delta\phi_n-\omega_0t=\alpha\int_0^t a_n(s)\,ds. \tag{21}$$

The clock therefore probes the area under the scalar transient. In the infinite-time limit, this is a low-frequency or DC response.

For the full microscopic two-sector modal system, two initial-condition protocols matter.

Zero fast-sector preparation. If the fast couplers begin unexcited, $x(0)=0$, and the scalar sector begins in a node mode with amplitude $a_n(0)$, then

$$\int_0^\infty a_n(t)\,dt=\frac{a_n(0)}{\mu^2+\lambda_n} \tag{22}$$

for every Ω in the linear model. Thus the integrated clock shift agrees with the Markovian static-gain prediction even when the instantaneous modal rate is badly distorted by finite-coupler memory or ringing.

Pre-equilibrated fast-sector preparation. If the fast sector begins at its adiabatic value, $x(0) = \Omega^{-1} HB\Lambda(0)$, then the area is no longer universally protected. For the uniform-fast-scale modal case, the relative clock-area error is

$$\frac{\left|\int a_n(t)dt - a_n(0)/(\mu^2 + \lambda_n)\right|}{|a_n(0)/(\mu^2 + \lambda_n)|} = \frac{\lambda_n}{\Omega}. \tag{23}$$

High modes and slow couplers can therefore produce large integrated timing errors.

Equations (22) and (23) are the corrected clock result. The clock channel is not "always true." It is robust for protocols that probe the static gain, including zero-fast-sector impulse-like preparations and slow/DC source changes, but it can fail for arbitrary fast-sector initial states, high-frequency drives, nonlinear edge variables, or measurements designed to resolve the ringing. In experimental language: rates are the strict dynamic closure test; clocks can be more robust because they integrate the load, but that robustness is protocol-dependent.

6 Numerical protocol

The revised numerical tests use full time-domain integrations of the coupled (Λ, x) system. For each graph and mode, the initial condition is a Laplacian eigenvector in the node sector. The edge sector is either set to zero or to its adiabatic value depending on the clock protocol being tested. The full linear system is evolved using matrix-exponential action on a vector. The node trajectory is projected back onto the chosen eigenmode. Small Gaussian readout noise is added to projected traces for the rate-recovery tests. Overdamped traces are fit to a two-exponential model; underdamped traces are fit to a damped sinusoid.

When sweeping the fast scale Ω, the simulations hold the generated weighted graph fixed. For target edge weight w_e, we set

$$g_e = h_e = \sqrt{w_e \Omega}, \tag{24}$$

so that $g_e h_e/\Omega = w_e$ remains constant while Ω changes the coupler response time. Without this scaling, changing Ω would change both the generated Laplacian and the fast-sector speed at once.

The test suite consists of five parts:

1. static Schur-complement closure;
2. full time-domain rate recovery across Ω for ring and star modes;
3. screening dependence of the ring/star first-mode ratio;
4. positive random edge-disorder tests;
5. clock-area tests comparing zero-fast-sector and pre-equilibrated-fast-sector protocols.

7 Results

7.1 Static closure

Static closure passed to numerical precision for 20-node ring and star graphs across $\Omega \in \{2, 5, 10, 50, 200\}$ with $\mu^2 = 0.05$. The maximum relative error between the full block-system steady state and the eliminated static closure was

$$8.76 \times 10^{-15}. \tag{25}$$

This verifies the Schur-complement implementation. It is not, by itself, independent evidence for scalar-selection.

7.2 Ring/star spectral separation and screening

For a 20-node ring and star with unit weights,

$$\lambda_1^{\text{ring}} = 2\left(1 - \cos\frac{2\pi}{20}\right) = 0.097887, \qquad \lambda_1^{\text{star}} = 1. \tag{26}$$

The weak-screening Markovian time-scale ratio is therefore

$$\frac{\tau_{\text{ring}}}{\tau_{\text{star}}} = \frac{\lambda_1^{\text{star}}}{\lambda_1^{\text{ring}}} = 10.216. \tag{27}$$

With $\mu^2 = 0.05$, the same ratio is

$$\frac{\tau_{\text{ring}}}{\tau_{\text{star}}} = \frac{\mu^2 + \lambda_1^{\text{star}}}{\mu^2 + \lambda_1^{\text{ring}}} = 7.100. \tag{28}$$

Thus the order-of-magnitude separation is a weak-screening result, not a universal graph-topological constant.

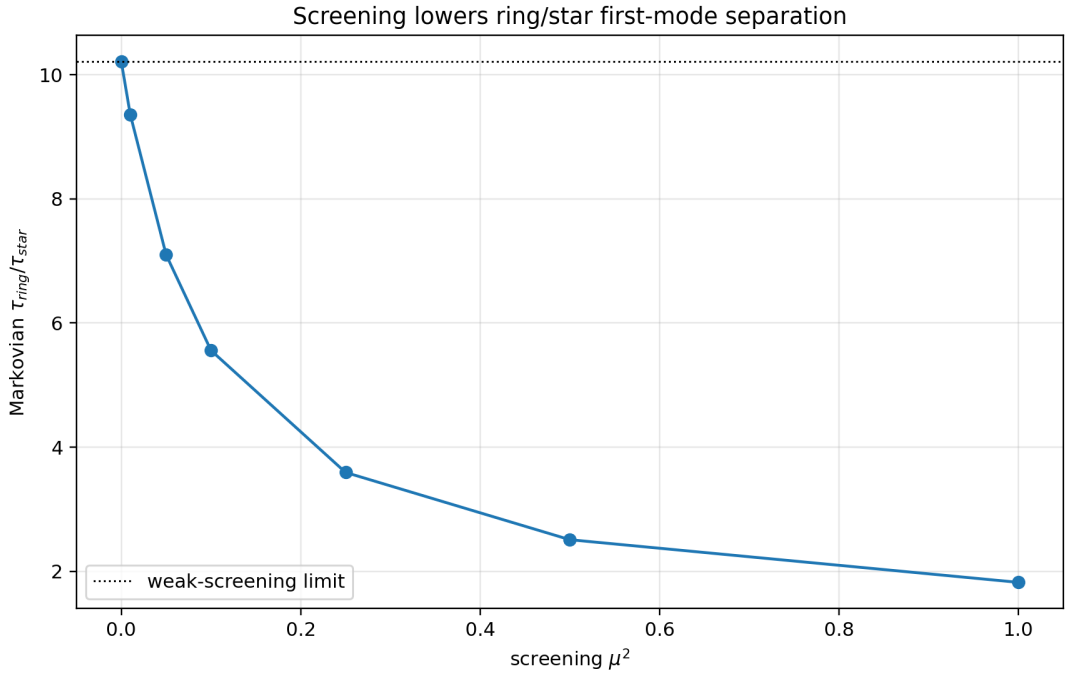

Figure 1: Screening lowers the ring/star first-mode relaxation-time separation. The 10.216 factor is recovered only as $\mu^2 \to 0$.

7.3 Noisy full time-domain rate recovery

Figure 2 summarizes fitted rates from noisy projected transients of the full coupled system. Low modes converge rapidly to the Markovian prediction as Ω grows. High modes show larger finite-coupler deviations because their λ_n values are closer to, or larger than, the fast-sector scale.

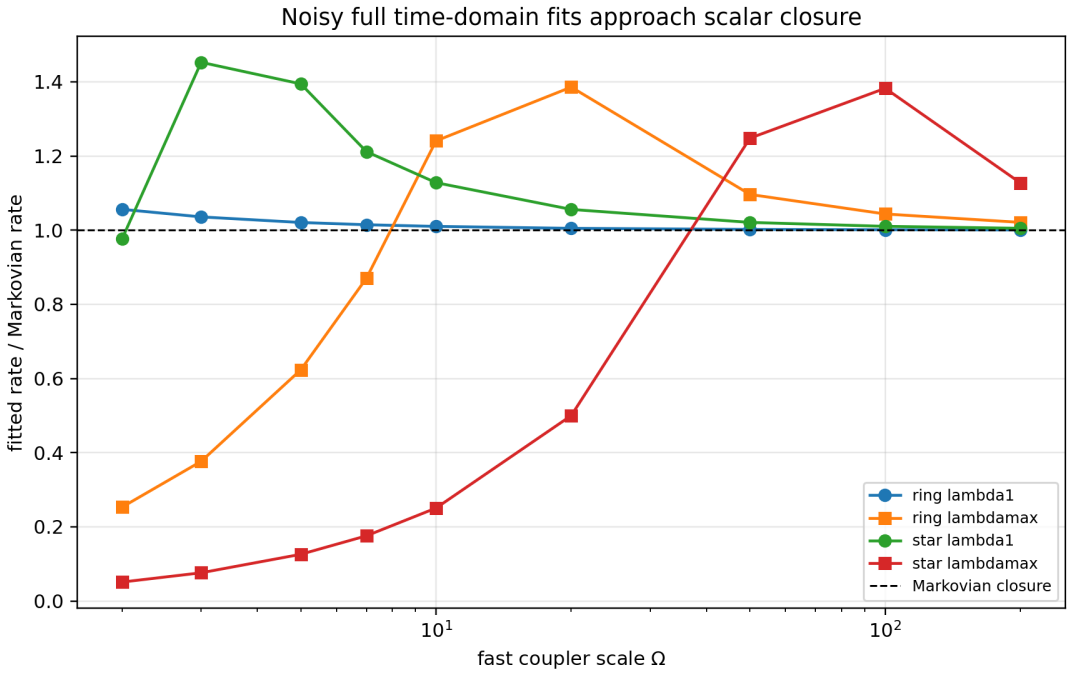

Figure 2: Noisy full time-domain fits approach the scalar-closure rate as Ω increases. The plotted rate is the fitted decay envelope divided by the Markovian prediction $\mu^2 + \lambda_n$.

The underdamped windows in Figure 3 follow Eq. (18). The star's high hub mode rings over the widest interval, whereas the first nonzero ring mode is underdamped only at very small Ω.

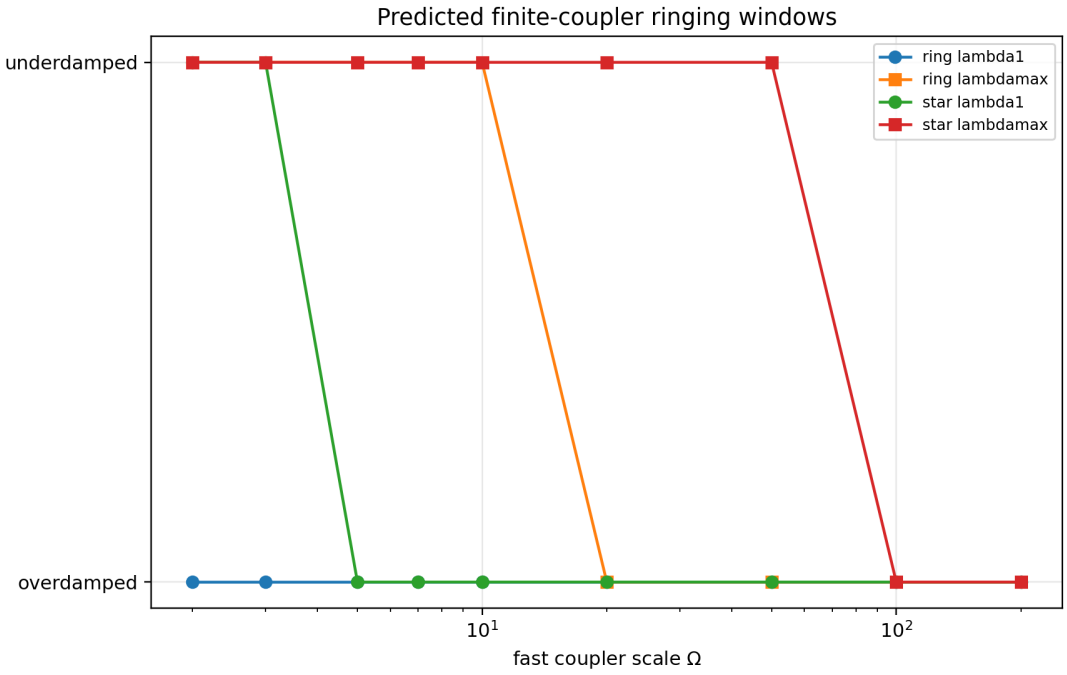

Figure 3: Finite-coupler ringing windows. High-λ modes enter underdamped behavior before low modes. This gives a mode-resolved failure signature rather than an undifferentiated mismatch.

Representative time-domain traces are shown in Figure 4. These are full-system integrations projected onto selected Laplacian modes, with small added readout noise.

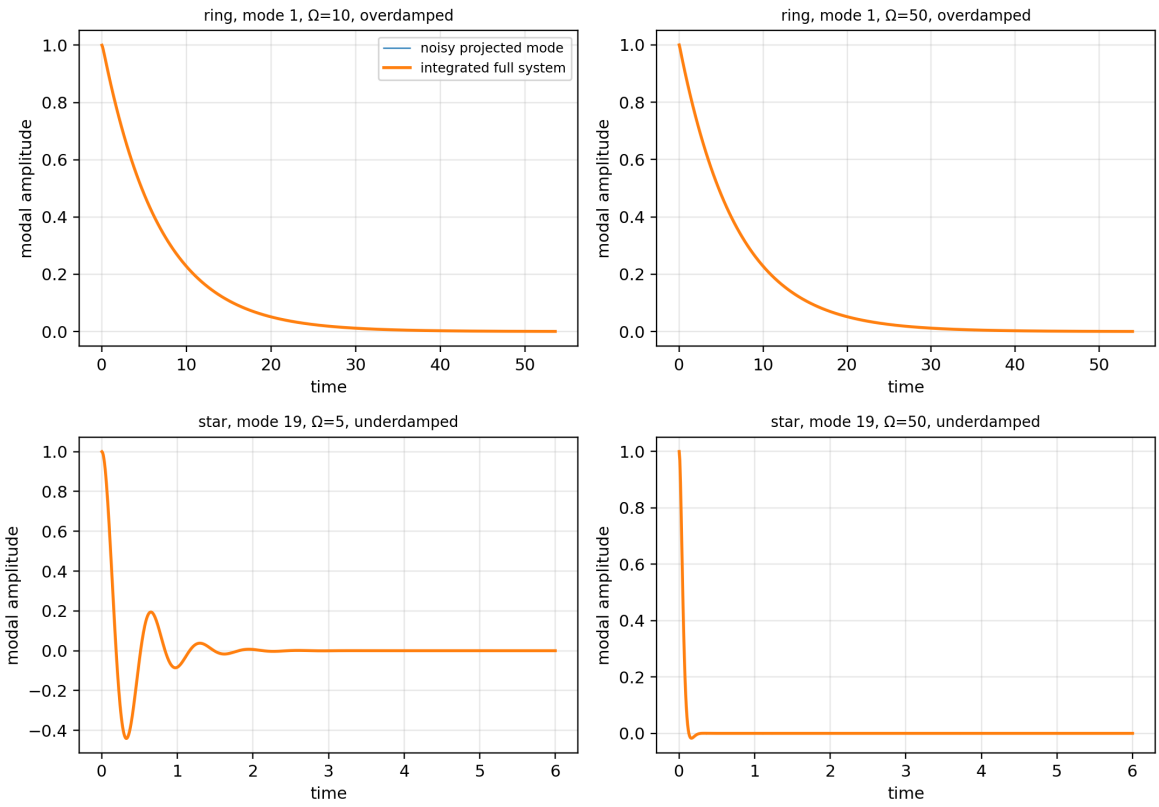

Figure 4: Representative full-system modal traces. The star high mode shows the expected finite-coupler oscillatory behavior at moderate Ω, while adiabatic cases decay cleanly.

7.4 Clock-area closure and protocol dependence

Figure 5 compares the integrated clock-area error for zero-fast-sector and pre-equilibrated-fast-sector protocols. The zero-fast-sector area agrees with the Markovian static-gain prediction to numerical precision across the sweep. The pre-equilibrated protocol follows the predicted λ_n/Ω error. This directly corrects the too-strong claim that frequency closure is always true.

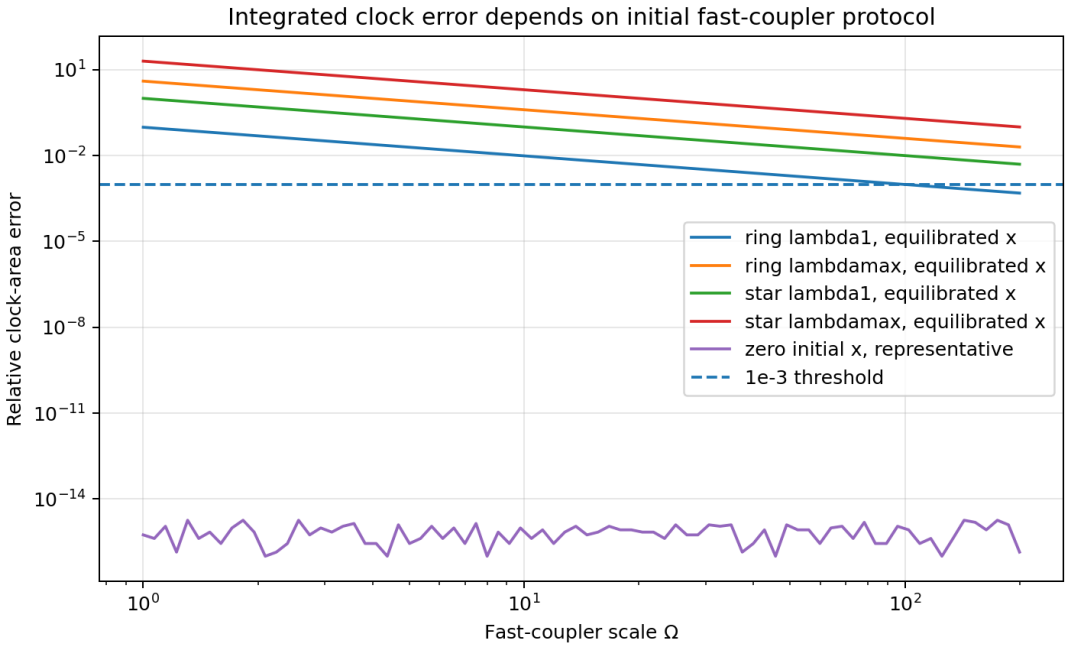

Figure 5: Clock-area error depends on preparation protocol. With $x(0) = 0$, the integrated scalar load matches the Markovian static gain for all Ω in the linear model. With pre-equilibrated fast variables, the area error scales as λ_n/Ω and can be large for high modes.

Table 1 gives representative values for selected modes at $\mu^2 = 0.05$. The star high mode has $\lambda_{\max} = 20$, so pre-equilibrated clock-area errors remain large unless $\Omega \gg 20$. By contrast, the zero-fast-sector clock-area error is machine-zero even when rate closure is poor.

Table 1: Selected clock-area errors. The zero-fast-sector protocol probes static gain; the pre-equilibrated protocol exposes the λ/Ω memory error.

Graph	Mode	λ	Ω	zero-x area err.	equil.-x area err.
Ring	λ_1	0.097887	1	0	0.097887
Ring	$\lambda_{\max}$	4.000000	10	3.4×10^{-16}	0.409019
Star	λ_1	1.000000	10	0	0.102255
Star	$\lambda_{\max}$	20.000000	10	1.4×10^{-16}	2.045094
Star	$\lambda_{\max}$	20.000000	50	1.4×10^{-16}	0.409766
Star	$\lambda_{\max}$	20.000000	200	0	0.100000

A representative high-mode microscopic trace is shown in Figure 6. In this regime, the rate observable is strongly affected by finite-coupler oscillations. Whether the clock area is protected depends on how the fast sector is prepared and what frequency band the measurement emphasizes.

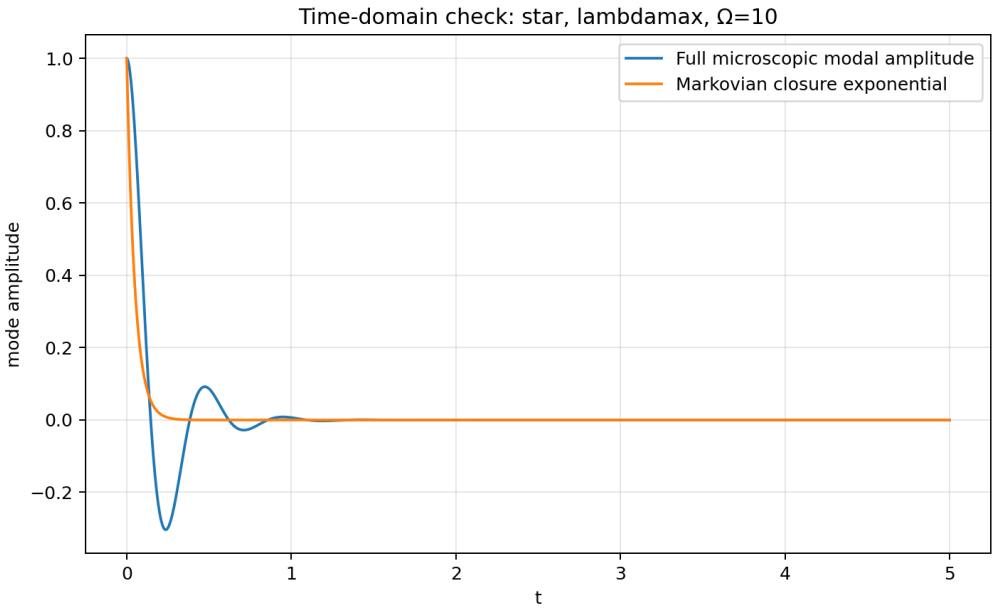

Figure 6: Star high-mode full microscopic trajectory at $\Omega = 10$. The finite coupler sector produces oscillatory behavior; dynamic rate closure fails strongly even though the zero-fast-sector integrated clock area remains equal to the static-gain prediction.

7.5 Positive edge-disorder tracking

A stronger check is to perturb the microscopic edge weights. If L_w is generated by the edge couplers, then changing $w_e = g_e h_e/\Omega_e$ should change the weighted spectrum, and the time-domain rates should track the changed spectrum. We tested noisy full-system transients on weighted rings and weighted chorded cycles with positive lognormal edge disorder.

Table 2: Noisy time-domain disorder tracking at $\Omega = 50$ and $\mu^2 = 0.05$. The measured rates are fitted from full microscopic transients, not directly read from analytic roots.

Graph family	Fits	R^2 vs closure	Mean rel. err. vs closure	Mean fit R^2
Weighted chorded cycle	16	0.999834	0.029604	0.999994
Weighted ring	16	0.999901	0.017310	0.999995

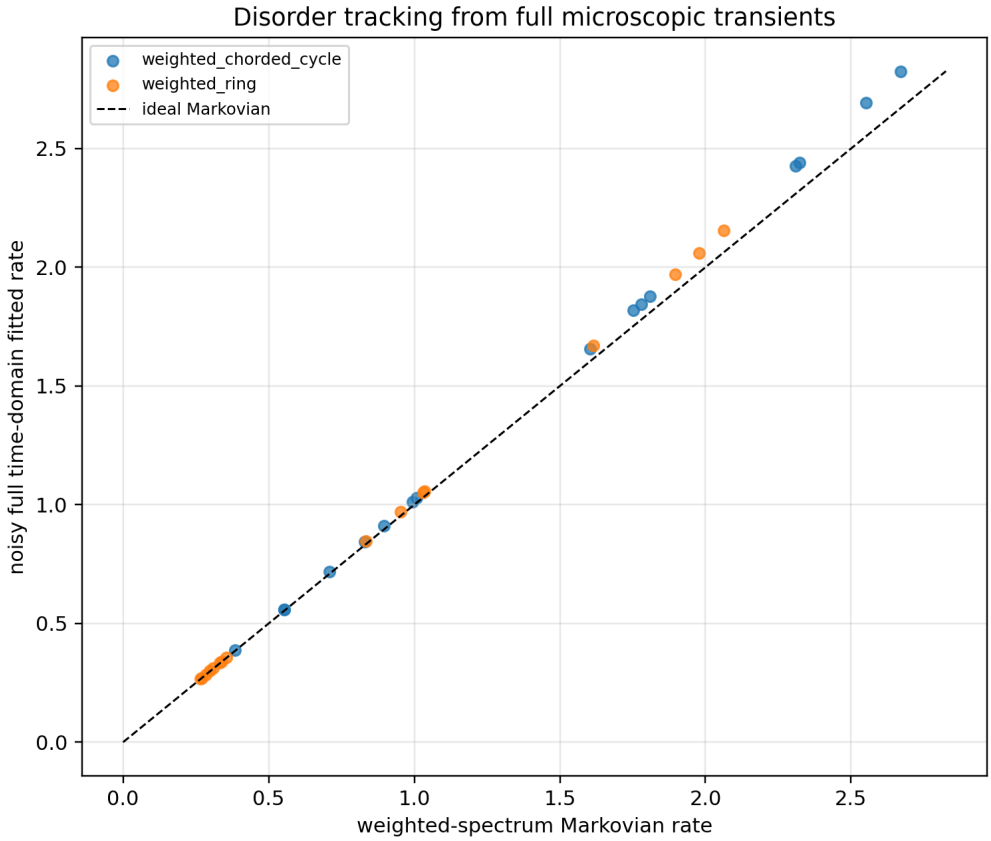

Figure 7: Disorder tracking from noisy full microscopic transients. Random positive edge weights change the weighted spectrum, and fitted modal rates track the new spectrum.

The residual errors relative to the Markovian closure are finite-coupler errors at $\Omega = 50$. The fitted rates match the exact full-system slow roots much more tightly, with mean relative errors below 2×10^{-4} in these tests. This is the expected hierarchy: the full microscopic model predicts the transients most accurately; the scalar closure is its large-Ω reduction.

8 Interpretation

The results support a narrow, disciplined conclusion.

1. The scalar response operator can be generated by eliminating microscopic edge variables on a specified substrate graph.
2. Static closure is algebraically necessary but not decisive.
3. Dynamic rate closure is the severe test, because it distinguishes adiabatic scalar behavior from finite-coupler memory.
4. Closure failure is structured: rate shifts and underdamped ringing occur in predictable graph-mode windows.
5. Clock observables introduce a weaker but important low-frequency closure: integrated phase can remain accurate even when modal rates fail, but only for protocols that probe static gain.

6. Edge disorder changes the generated weighted spectrum, and noisy full-system modal fits track that new spectrum.

The phrase "not inserted as an ansatz" should therefore be understood carefully. The substrate graph is specified by the medium architecture. What is not inserted directly is the scalar-response weight matrix; it arises from coupler parameters through the Schur complement. More precisely, this is a microscopic realization or network synthesis of a positive weighted Laplacian on a specified substrate graph, not a derivation of the graph topology itself.

The clock result is the main addition in this version. Scalar-selection is timing-first, so a rate-only paper would miss the observable distinction that matters most. The corrected message is not that timing always saves the closure. The corrected message is that rate closure and clock closure test different response functions. Rates probe poles. Integrated clocks probe static gain. These coincide in the adiabatic limit, but they can diverge at finite coupler speed.

9 Relation to experiments

The model is abstract but intentionally resembles reconfigurable coupled media. Superconducting circuits already use tunable and modular coupler architectures, and precision timing experiments already make extremely small frequency shifts measurable. Those facts motivate, but do not prove, experimental relevance. A first physical implementation would need to show that observed transients track the graph spectrum rather than thermal relaxation, electromagnetic pickup, microwave drive artifacts, mechanical vibration, or servo behavior.

The experiment suggested by this paper is therefore not a test of gravity. It is a first-bound internal-medium test: switch or program edge couplers, measure an internal phase/timing proxy, fit modal transients, and ask whether the relaxation spectrum follows L_w and the finite-coupler corrections derived here.

The clock analysis adds an experimental design criterion. If the goal is to observe clean Markovian exponential transients, operate in a regime with $\Omega \gg \lambda_{\max}$ for the modes excited. If the goal is to verify finite-coupler memory, deliberately excite high-λ modes where Eq. (18) predicts ringing. If the goal is to detect a stable timing shift, use slow or step-like protocols that probe static gain and control the initial fast-sector state.

10 Limitations

This paper has several limitations.

1. The model is linear and finite-dimensional.
2. The construction realizes a chosen substrate graph; it does not derive the graph topology or explain why a given architecture is selected.
3. The Laplacian form requires positive diagonal edge-coupler assumptions.
4. Non-diagonal, directed, sign-changing, and non-normal edge sectors are excluded.
5. For nonuniform fast scales, finite-coupler transients can depend on G, H, and Ω separately, even when the same static L_w is produced.
6. The static result follows by Schur complement and is confirmatory.

7. The time-domain tests are still simulations of the same linear model, not physical measurements or independent empirical evidence.

8. The clock channel is minimal. It does not include oscillator backreaction, readout bandwidth, feedback, phase noise, nonlinear clock coupling, or a full experimental servo model.

9. Integrated clock closure is protocol-dependent. It is robust for zero-fast-sector and low-frequency/DC protocols in this model, not for arbitrary initial fast-sector excitations or high-frequency measurements.

10. The result is internal to the medium. It does not establish an external coupling kernel $C(x, i)$.

11. No claim is made about external scalar geometry, gravitational redshift, Lorentz invariance, or spin-2 dynamics.

11 Next steps

The next useful simulations are: (i) replace the minimal clock channel with explicit oscillator degrees of freedom and finite-bandwidth phase readout; (ii) test non-diagonal and sign-indefinite coupler sectors to map the boundary of Laplacian closure; (iii) add nonlinear coupler saturation; (iv) add stochastic drive, colored noise, and servo feedback; (v) test larger generated weighted graphs for spectral-dimension closure; and (vi) model internal-to-external coupling kernels separately.

12 Conclusion

A minimal positive fast-coupler medium can realize the weighted graph Laplacian required by scalar-selection closure on a specified substrate graph. The result is a microscopic bridge, not a theory of gravity. Static closure passes because it is the Schur complement of the full block system. Dynamic rate closure is the strict test: the Markovian scalar rate is recovered only in the adiabatic regime, and finite-coupler corrections produce predictable rate shifts and underdamped high-mode ringing.

Adding a clock channel sharpens the significance of the result. The scalar load may produce robust integrated timing shifts even when modal rate closure fails, because phase integrates the low-frequency scalar response. But this robustness is not universal; it depends on the fast-sector preparation and measurement protocol. The final picture is therefore two-tiered: rate observables expose finite-coupler memory, while DC or integrated clock observables can remain governed by the static weighted Laplacian.

The appropriate interpretation is conservative: this model makes the scalar-selection operator less ad hoc and supplies quantitative validity and failure criteria. That is enough for a narrow results paper, and not more than enough.

A Reproducibility details for the numerical tests

All graphs in the reported tests use $N = 20$ nodes. The ring has edges $(i, i + 1 \bmod 20)$. The star has hub node 0 and leaf edges $(0, i)$ for $i = 1, \ldots, 19$. The unit ring and star use $w_e = 1$. For weighted-disorder tests, positive lognormal weights are sampled first, then held fixed while fitting modes at $\Omega = 50$ and $\mu^2 = 0.05$.

For each selected Laplacian eigenvector ϕ_n, the node initial condition is

$$\Lambda(0) = \phi_n. \tag{29}$$

For rate tests, unless otherwise stated, the edge sector begins at $x(0) = 0$. For clock-area protocol tests, both $x(0) = 0$ and $x(0) = \Omega^{-1} HB\Lambda(0)$ are tested. The full block generator from Eq. (14) is evolved, and the scalar trace is projected as

$$a_n(t) = \phi_n^T \Lambda(t). \tag{30}$$

Gaussian readout noise is added at a small amplitude relative to the trace scale for the noisy rate-recovery tests. Overdamped traces are fit using a two-exponential model because setting the edge variables initially to zero excites both the fast and slow roots. Underdamped traces are fit by a decaying sinusoid plus a small offset. Fits with poor numerical conditioning or insufficient signal are discarded before computing summary statistics.

The comparison hierarchy is:

1. fitted time-domain rate versus exact full microscopic slow root;
2. fitted time-domain rate versus Markovian closure rate $\mu^2 + \lambda_n$;
3. integrated clock area versus Markovian static gain $1/(\mu^2 + \lambda_n)$;
4. Markovian closure rate versus graph spectrum under changes of weights.

The first comparison checks recovery from noisy transients. The second measures finite-Ω error. The third separates protocol-protected timing from memory-sensitive timing. The fourth checks whether weight disorder changes recovered rates through the generated weighted spectrum.

Data and code availability

The package accompanying this draft includes CSV files for static closure errors, graph spectra, time-domain modal fits, screening ratios, underdamped intervals, clock-area sweeps, and disorder tracking, along with the figures used in the paper. The simulation harness is independent of earlier QATNU exact-diagonalization scripts.

References

[1] A. N. Tikhonov, "Systems of differential equations containing small parameters in the derivatives," *Matematicheskii Sbornik* **31**, 575–586 (1952).

[2] P. V. Kokotovic, H. K. Khalil, and J. O'Reilly, *Singular Perturbation Methods in Control: Analysis and Design*, Academic Press (1986).

[3] H. A. Simon and A. Ando, "Aggregation of variables in dynamic systems," *Econometrica* **29**, 111–138 (1961).

[4] F. Zhang, editor, *The Schur Complement and Its Applications*, Springer (2005).

[5] F. R. K. Chung, *Spectral Graph Theory*, American Mathematical Society (1997).

[6] B. Bollobas, *Modern Graph Theory*, Springer (1998).

[7] R. Burioni and D. Cassi, "Universal properties of spectral dimension," *Physical Review Letters* **76**, 1091–1093 (1996).

[8] F. Chung and S.-T. Yau, "Discrete Green's functions," *Journal of Combinatorial Theory, Series A* **91**, 191–214 (2000).

[9] G. Calcagni, D. Oriti, and J. Thurigen, "Spectral dimension of quantum geometries," *Classical and Quantum Gravity* **31**, 135014 (2014).

[10] J. Stehlik et al., "Tunable coupling architecture for fixed-frequency transmon superconducting qubits," *Physical Review Letters* **127**, 080505 (2021).

[11] X. Jin et al., "Versatile parametric coupling between two statically decoupled transmon qubits," *Physical Review Applied* **19**, 064043 (2023).

[12] M. Field et al., "Modular superconducting-qubit architecture with a multichip tunable coupler," *Physical Review Applied* **21**, 054063 (2024).

[13] T. Bothwell et al., "Resolving the gravitational redshift across a millimetre-scale atomic sample," *Nature* **602**, 420–424 (2022).

[14] S. Kono et al., "Mechanically induced correlated errors on superconducting qubits with relaxation times exceeding 0.4 ms," *Nature Communications* **15**, 4500 (2024).